Density functional study on chirospectra of hydrogen-bonded systems $X^-(H_2O)_3$ (X = F, Cl, Br, I)*

Mang Chao-Yong(莽朝永)[a)b)†], Li Zhen-Gui(李珍贵)[a)], and Wu Ke-Chen(吴克琛)[c)‡]

[a)] *College of Life Science and Chemistry, Dali University, Dali* 671000, *China*
[b)] *Institute of Eastern-Himalaya Biodiversity Research, Dali University, Dali* 671000, *China*
[c)] *State Key Laboratory of Structural Chemistry, Fujian Institute of Research on the Structure of Matter, Chinese Academy of Sciences, Fuzhou* 350002, *China*

(Received 3 March 2009; revised manuscript received 1 June 2009)

This paper calculates the molecular structures, infrared, Raman, circular dichroism spectra and optical rotatory powers of some hydrogen-bonded supramolecular systems as a cyclic water trimer, $(H_2O)_3$ and its pyramidal halide complexes, $X^-(H_2O)_3$ (X = F, Cl, Br, I) with the gradient-corrected density functional theory method at the B3LYP/6–311++G(2d,2p) and B3LYP/Aug–cc–pVTZ levels. It finds that the complexation of halide anions with the water trimer can efficiently modulate the chirally optical behaviors. The calculated vibrational circular dichroism spectrum illuminates that the vibrational rotational strength of S(+)–$(H_2O)_3$ mostly originates from the O–H rocking modes, whereas chirality of S(–)–$X^-(H_2O)_3$ (X = F, Cl, Br, I) has its important origin in the O–H stretching modes. The calculated optical rotatory power demonstrates that S(+)–$(H_2O)_3$ and S(+)–$F^-(H_2O)_3$ are positively chiral, whereas S(–)–$X^-(H_2O)_3$ (X = Cl, Br, I) are negatively chiral. With the polarizable continuum model, calculated bulk solvent effect in the solvents water and carbontetrachloride and argon shows that the positive chirality of S(+)–$(H_2O)_3$ is enhanced and the negative chirality of S(–)–$X^-(H_2O)_3$ (X = Cl, Br, I) and the positive chirality of S(+)–$F^-(H_2O)_3$ are reduced with an augmentation of the solvent dielectric constant.

Keywords: water cluster, hydrogen-bond, vibrational circular dichroism, infrared spectra, density functional theory

PACC: 3640, 7115M

1. Introduction

As a result of the lengthy selections of chirality, enantiomers such as L amino-acids and D single-sugars survive in nature. Currently, research on chirality has become a significant subject since different chiral isomers of some medicines, pesticides, health foodstuffs and cosmetics probably exhibit different bioactivity through the interactions with other chiral biomacromolecules such as proteins and nucleotides as well as DNA, along with the events of chiral recognitions frequently entangled in life systems.

Although the water monomer is absent of chirality, some water clusters become chiral through supramolecular self-assemblies. For example, the quantum tunneling technique has detected that the six-numbered-ring water trimer is chiral.[1] Since the Nobel Prize for Chemistry in 2003 was awarded for the discovery of the channels of water and potassium ions in cell membrane, it has become gradually understood that small water clusters are important in the metabolism process of water, nourishment, and waste in cells. Compared with a large water cluster, a small water cluster can more readily penetrate the cell membrane, maintain a high percentage of water and an effective hydration interaction in the cell, and help restore health, youth, and vigor.

The unique functions of small water clusters have urged scientists to design novel bulk structural water composed of small water clusters with special functions. Next, the studies of chiral assembly of water molecules are helpful for a better understanding of the foundational interactions between water and organisms and easier design of novel functional water products. For small water clusters up to pentamers, it has been proven that the cyclic structures are the most stable.[2,3] Furthermore, a great numbers of investigations have been given to ion-hybrid water clusters such

*Project supported by the Scientific Foundation of Education Department of Yunnan Province of China (Grant No. 07Z11621), the Innovation Foundation for New Researchers in Dali University (Grant No. KY421040), and the National Natural Science Foundation of China (Grant No. 20573114).

†Corresponding author. E-mail: cymang@gmail.com
‡E-mail: wkc@fjirsm.ac.cn

© 2010 Chinese Physical Society and IOP Publishing Ltd

as halide-water clusters $X^-(H_2O)_n$ (X = F, Cl, Br, I)[4−8] and alkali-metal-water clusters $M^+(H_2O)_n$ (M = Li, Na, K, Rb, Cs)[9−12] as well as neutral species such as benzene-$(H_2O)_n$[13,14] clusters and ethanol-water clusters.[15] Apparently, the hydrogen-bonded interactions are motors of the self-reassembly of water molecules in these clusters.

The circular dichroism (CD) spectra and the optical rotatory power (ORP) are often used to determine absolute configuration (AC) of optical active molecules. The CD spectra are classified as vibrational CD (VCD) spectra and electronic CD (ECD) spectra, where an enantiomeric pair respectively exhibits the positive and negative absorptions at the same wavelengths referred to as the positive and negative Cotton effects. The ORP is often measured at the incident light of the sodium D-line, 598 nm at 20 °C, where an enantiomeric pair possesses equal values of opposite sign. Theoretically, Alkorta and Elguero *et al.* have investigated the chirally recognizable events of some hydrogen-bonded cluster isomers of hydrogen peroxide,[16,17] diaziridine,[18] and oxiranes.[19] In the present work, the chiroptical properties of the $(H_2O)_3$ and $X^-(H_2O)_3$ (X = F, Cl, Br, I) clusters, containing ORP and VCD spectra, are characterized at the molecular orbital level of the density functional theory (DFT), along with the prediction of infrared (IR) and Raman spectra.

2. Computational methodology

Some low-energy isomers of S–$(H_2O)_3$ and S–$X^-(H_2O)_3$ (X = F, Cl, Br, I) without symmetry constraint are optimized by means of the gradient-corrected density functional theory (DFT) method at B3LYP/6–311++G(2d,2p) and B3LYP/Aug–cc–pVTZ levels (Table 1 and Fig. 1). Here B3LYP is a well-defined hybrid functional containing Becke's three parameter exchange functions,[20] non-local correlation functions of Lee–Yang–Parr (LYP),[21,22] and local correlation of Vosko–Wilk–Nusair (VWN).[23] The basis set 6–311++G(2d,2p) is an all-electron triple-zeta split valence basis extended by polarization and diffuse functions[24−26] in the molecular orbital approximations of 6s2p/4s2p for H, 12s6p2d/5s4p2d for O and F, 13s10p2d/6s4p2d for Cl, 15s13p7d/8s7p4d for Br. Aug–cc–pVTZ is also a larger all-electron triple-zeta split valence basis by containing more polarization and diffuse functions[27−31] as 6s3p2d/4s3p2d for H, 11s6p3d2f/5s4p3d2f for O and F, 16s10p3d2f/6s5p3d2f for Cl, 21s14p10d2f/7s6p4d2f for Br, 13s12p10d2f/6s5p4d2f namely, called Aug–cc–pVTZ-pp[32] for I.

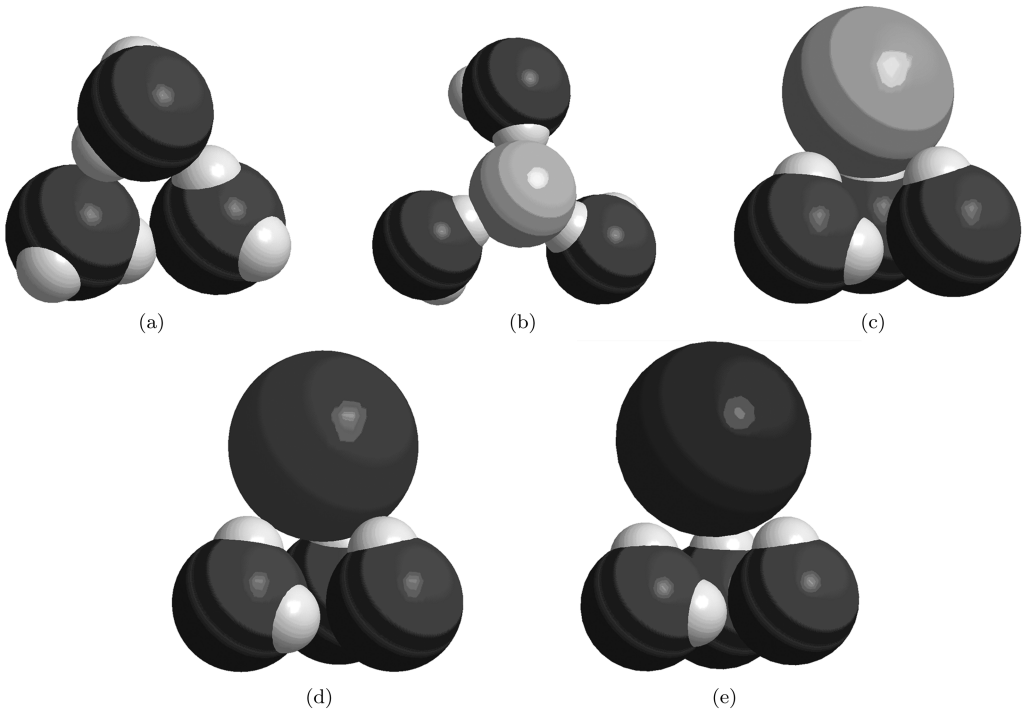


Fig. 1. Space filling maps of optimized S-enantiomer of S(+)–$(H_2O)_3$ (a), S(+)–$F^-(H_2O)_3$ (b), and S(–)–$X^-(H_2O)_3$ (X = Cl, Br, I) (c–e).

Table 1. Optimized bond distances (in Å, 1 Å = 0.1 nm), bond angles (in degrees), Mulliken change density of halide (Q), frequency distance ($\Delta\nu$ in cm^{-1}) between the OH_{bw} and OH_{bx} (OH_f) stretching.

	O1O2	O2O3	O3O1	OH_{bw}	OH_{bx}	O1X	O2X	O3X	OOO	OXO	$-Q$	$\Delta\nu$
S(+)–$(H_2O)_3$					(OH_f)							
B3LYP/6–311++G(2d,2p)	2.803	2.804	2.810	0.975	0.960				59.9∼60.2			300
B3LYP/Aug–cc–pVTZ	2.803	2.804	2.810	0.976	0.961				59.9∼60.2			
MP2/6–311+G**[38]	2.789	2.793	2.801	0.970	0.958							
MP2/Aug–cc–pVDZ[2]	2.798	2.799	2.800	0.978	0.964							
S(+)–$F^-(H_2O)_3$												
B3LYP/6–311++G(2d,2p)	4.282	4.283	4.284	0.960	1.000	2.602	2.601	2.602	60.0	110.8	0.725	746
B3LYP/Aug–cc–pVTZ	4.294	4.295	4.300	0.960	1.002	2.591	2.590	2.588	59.9∼60.1	112.1	0.803	
MP2/6–311++G**[4]				0.958	0.995	2.582						
MP2/TZ(2df,2pd)++[39]					0.995	2.599						
MP2/Aug–cc–pVDZ[40]	3.247			0.967	1.000	2.610	2.610	2.610				
S(–)–$Cl^-(H_2O)_3$												
B3LYP/6–311++G(2d,2p)	3.002	3.003	3.003	0.969	0.978	3.229	3.228	3.230	60.0	55.4	0.831	185
B3LYP/Aug–cc–pVTZ	3.027	3.028	3.028	0.969	0.979	3.233	3.232	3.234	60.0	55.8	0.926	
MP2/6–311++G**[39]					0.974	3.211						
MP2/TZ(2df,2pd)++[39]					0.978	3.166						
MP2/Aug–cc–pVDZ[5]	3.010			0.974	0.982	3.223						
S(–)–$Br^-(H_2O)_3$												
B3LYP/6–311++G(2d,2p)	3.002	3.004	3.005	0.969	0.975	3.427	3.426	3.430	59.9∼60.1	52.0	0.882	108
B3LYP/Aug–cc–pVTZ	3.007	3.008	3.010	0.970	0.976	3.431	3.430	3.431	60.0	52.0	0.970	
MP2/6–311++G**[39]					0.972	3.403						
S(–)–$I^-(H_2O)_3$												
B3LYP/6–311++G(2d,2p)	2.950	2.951	2.954	0.972	0.972	3.704	3.696	3.707	59.9∼60.1	47.0	0.920	70
B3LYP/Aug–cc–pVTZ	3.015	3.019	3.021	0.970	0.974	3.695	3.681	3.696	59.9∼60.1	48.2	0.825	
MP2/6–311++G**[39]					0.969	3.700						
MP2/Aug–cc–pVDZ+diff[6]				0.972	0.974	3.69						

Note: H_{bw}, hydrogen-bonded combination with another water, H_{bx}, hydrogen-bonded combination with halide X, and H_f, free dangling H.

According to harmonic frequency calculations, no imaginary frequency is found, indicating that all optimized geometries are the true minima. The IR intensity (I), vibrational rotation strength (R) and Raman activity (A) are calculated on the basis of optimized geometry. In all calculations, the Gaussian 03 program[33] was adopted, containing tight self-consistent field (SCF) convergences as 10^{-7} Hartree for the total energy threshold and 10^{-6} au/Bohr for gradient correction.

The ORP, $[\alpha]_D$ at the incident light wavelength of the sodium D-line and $[\alpha]_{D0}$ at zero frequency, are calculated in terms of summed equations of the optical rotatory strengths,[34,35]

$$\beta(\omega) = \frac{2c}{3}\sum_{\lambda}\frac{R_{0\lambda}}{\omega_{0\lambda}^2 - \omega^2}, \tag{1}$$

$$[\alpha]_\omega = 7200\frac{\omega^3 N_A}{c^2 M}\beta(\omega), \tag{2}$$

where $\beta(\omega)$ is the optical rotation parameter, $R_{0\lambda}$ is the optical rotation strength for $0 \to \lambda$ excitation, ω is the frequency of incident polarized light, $\omega_{0\lambda}$ is the vertical transition frequency, M is the molecular molar weight, N_A is Avogadro's number, and c is a constant equal to 137.036 in dimensionless atomic units. $R_{0\lambda}$ is calculated by the imaginary part of point multiplication of electric and magnetic transition dipole moments,

$$R_{0\lambda} = \mathrm{Im}(\boldsymbol{\mu}_{0\lambda} \cdot \boldsymbol{m}_{0\lambda}). \tag{3}$$

The solvent effect in water and CCl_4 and Ar is simulated with the polarizable continuum model (PCM) method presented by Tomas and coworkers,[36] where the dielectric constant utilized is 78.79 F/m for water, and 2.228 F/m for CCl_4, and 1.43 F/m for Ar. Selected results were shown in Tables 1–4 and Figs. 1 and 2.

3. Results and discussion

3.1. Absolute configuration (AC)

Recently, Zhang *et al.*[37] addressed the cyclic structure of $(H_2O)_3$ by means of the single-parent genetic algorithm, showing that the six-numbered-ring structure possesses the lowest energy. In our present work, the lowest structure of this cluster also is cyclic through the hydrogen-bonded interactions. Almost the same geometric parameters of AC of cyclic S–$(H_2O)_3$ are predicted at B3LYP/6–311++G(2d,2p) and B3LYP/Aug–cc–pVTZ. The optimized three O–O bonds are 2.803, 2.804, and 2.810 Å (1 Å = 0.1 nm), respectively (Table 1). Furthermore, the O1O2O3 and O2O3O1 angles are optimized to be 59.9°, and the O3O2O1 is 60.2°. Thus, three oxygen atoms establish a quasi-equilateral triangle. The mean O–O length (2.806 Å) is a little longer than those previously reported, 2.794 Å at MP2/6–311+G**,[38] and 2.799 Å at MP2/Aug–cc–pVDZ.[2] The optimized O–H_{bw} (H_{bw}, hydrogen-bonded combination with another water) and O–H_f (H_f, free dangling H) distances are close to those at MP2/6–311+G** and MP2/Aug–cc–pVDZ. Therefore, comparison with the MP2 calculations shows that the present optimized geometries at the DFT level are acceptable.

Optimized S–$F^-(H_2O)_3$ has a quasi-planar feature. The averaged O–O distance (4.283 Å) at B3LYP/6–311++G(2d,2p) is slightly shorter than that (4.296 Å) at B3LYP/Aug–cc–pVTZ, and closer to the value (4.247 Å) at MP2/Aug–cc–pVDZ.[5] As a result of water-fluorine strong interactions, the hydrogen bonds between water molecules are apparently weakened to a great tendency. According to the analysis of Mulliken charge population at B3LYP/6–311++G(2d,2p), the charge density of the fluorine in this complex is −0.725. In other words, 0.275 electrons are transferred to water molecules. Therefore, $F^-(H_2O)_3$ is a typical charge-transferred species.

The optimized O–H_{bx} (H_{bx}, hydrogen-bonded connection with X) and O–H_{bw} distances are in the range of magnitudes at MP2/TZ(2df,2pd)++[39] and MP2/Aug–cc–pVDZ.[40] The averaged O–F distance (2.602 Å) is close to those at the MP2 level, 2.582 Å at MP2/6–311++G**,[4] 2.599 Å at MP2/TZ(2df,2pd)++,[39] and 2.610 Å at MP2/Aug–cc–pVDZ.[40] The molecular structure takes on a quasi-planar feature in the light of the OXO angels, 112.0° at B3LYP/6–311++G(2d,2p) and 110.8° at B3LYP/Aug–cc–pVTZ. Due to the strong hydrogen-bond interactions between fluorine and water, the O–H_{bx} bond is extended (1.000 Å, but O–H_f, 0.960 Å), and results in a very low stretching frequency (2984 cm^{-1}). As a direct result of the red shift of this stretching frequency, the frequency gap between the O–H_{bw} and O–H_{bx} stretching vibrations is rather largely widened (746 cm^{-1} in Table 1).

The optimized molecular skeleton of S–$Cl^-(H_2O)_3$ is close to a pyramidal structure. The averaged O–O distance at B3LYP/6–311++G(2d,2p) (3.003 Å) is a little shorter than those at B3LYP/Aug–cc–pVTZ (3.028 Å) and at MP2/Aug–cc–pVDZ (3.010 Å).[5] The averaged O–Cl distance, 3.229 Å at B3LYP/6–311++G(2d,2p) and 3.233 Å at B3LYP/Aug–cc–pVTZ, is a little longer than those at the MP2 level, 3.211 Å at MP2/6–311++G**,[41] 3.166 Å at MP2/TZ(2df,2pd)++,[41] and 3.223 Å at MP2/Aug–cc–pVDZ.[5] Three oxygen atoms almost form an equilateral triangle and the halide-water complex is close to a standard pyramid (Fig. 1(c)). In this complex, chlorine has –0.831e at B3LYP/6–311++G(2d,2p), with a smaller magnitude of charge transfer in comparison with the above-mentioned fluorine-water species. Due to the weaker water-halide interactions, the O–H_{bw} and O–H_{bx} stretching frequency difference (185 cm^{-1}) is much smaller.

For the pyramidal structure of S–$Br^-(H_2O)_3$, the averaged O–O distance (3.004 Å) is almost the same as that in S–$Cl^-(H_2O)_3$, 3.003 Å at B3LYP/6–311++G(2d,2p). The O–Br distance, 3.426 Å at B3LYP/6–311++G(2d,2p) and 3.430 Å at B3LYP/Aug–cc–pVTZ is a little longer than that (3.403 Å) at MP2/6–311++G**.[39] The charge density of bromine is –0.831 at B3LYP/6–311++G(2d,2p), with a smaller charge transfer than S–$Cl^-(H_2O)_3$.

For pyramidal S–$I^-(H_2O)_3$, the O–O distance is the shortest in these halide-water complexes, implying that the water-halide interactions are the weakest and almost fail to influence the water-trimer structure. Furthermore, the O–X distance (2.952 and 3018 Å) at the DFT level is longer than that in other complexes. The results at the DFT level are close to those at the MP2 level. For example, the averaged O–I distance, 3.702 Å at B3LYP/6–311++G(2d,2p) and 3.691 Å at B3LYP/Aug–cc–pVTZ, is in agreement with that at MP2 level, 3.700 Å at MP2/6–311++G**[40] and 3.69 Å at MP2/Aug–cc–pVDZ+diff.[6] The charges of iodine are predicted to be –0.920e at B3LYP/6–

311++G(2d,2p), showing the least charge transfer. The OXO angle is reduced with addition of the halide radius. As a result, this complex possesses the smallest OXO angle (47°). In addition, the O–H_{bw} and O–H_{bx} stretching frequency difference (70 cm^{-1}) is also the smallest.

3.2. Vibrational circular dichroism (VCD)

The DFT method is frequently used to determine the structures and harmonic vibrational frequencies of the metal clusters,[41,42] showing many successes in recent years. As we know, this method is a powerful tool to predict the IR spectra. In 1980, Bentwood *et al.* experimentally measured the IR spectrum of cyclic $(H_2O)_3$,[43] however, these vibrational frequencies have not been well assigned. In Fig. 2(a), we notice that three strong absorption peaks appear at about 1590, 3485, 3738 cm^{-1}, respectively. In Table 2, we assigned the experimental vibrational peaks to the ν_{13}–ν_{21} normal vibrational modes. The ν_{13}–ν_{15} modes are associated with the HOH bending, the ν_{16}–ν_{18} modes are the O–H_{bw} stretching, and the ν_{19}–ν_{21} modes originate from the O–H_f stretching, suggesting that these vibrations cause the changes of the dipole moment of this cluster. Of them, the ν_{16}–ν_{21} modes are Raman-active, proposing that these vibrations lead to the alterations of the dipole polarizability of the system. Furthermore, ν_{17} exhibits the largest IR-activity, and ν_{16} has the strongest Raman-activity. Calculated frequencies (1589–3740 cm^{-1}) at B3LYP/6–311++G(2d,2p) are smaller than those (1632–3898 cm^{-1}) at MP2/Aug–cc–PVDZ reported by Xantheas and Dunning,[2] where the latter uniformly overestimates the experimental values (1602–3703 cm^{-1}).[41] Compared with the values at the MP2 level, we find that the results at the B3LYP level are much closer to the experimental data. More concretely, the ν_{13}–ν_{18} modes have some underestimates compared to the experimental data, and the ν_{19}–ν_{21} modes exhibit a few overestimates.

Table 2. Harmonic vibration frequency (ν, in cm^{-1}), infrared intensity (I, in kM/mol), Raman activity (A, in $Å^4$/a.u.), and vibrational optical rotatory strength (R, in $\times 10^{-40}$ $esu^2 \cdot cm^2$) of S(+)–$(H_2O)_3$ and S(+)–$F^-(H_2O)_3$ calculated at the B3LYP/6–311++G(2d,2p) level, where the harmonic frequency has been scaled by a scaling factor of 0.962.

	S(+)–$(H_2O)_3$						S(+)–$F^-(H_2O)_3$			
mode	ν	MP2[a]	Expt[43]	I	A	R	ν	I	A	R
ν_1	173	158		15	0	32	19	1	0	–4
ν_2	178	173		10	0	–1	24	1	0	–4
ν_3	198	185		123	0	19	25	1	0	–4
ν_4	211	193		19	0	–41	114	47	0	–131
ν_5	215	218		127	0	–71	125	48	0	–135
ν_6	254	235		52	0	37	168	162	0	237
ν_7	344	343		70	0	–90	242	2	0	0.86
ν_8	357	351		36	0	240	280	58	0	13
ν_9	442	444		130	0	–31	280	59	0	12
ν_{10}	572	571		190	0	–110	465	64	0	163
ν_{11}	658	667		325	0	–56	473	71	2	–83
ν_{12}	861	863		9	0	125	475	71	2	–76
ν_{13}	1589	1632	1602	84	2	–16	874	68	3	–90
ν_{14}	1592	1635	1620	78	2	–45	878	68	3	–94
ν_{15}	1612	1660	1632	15	1	25	887	166	0	202
ν_{16}	3419	3573	3517	13	252	–10	1638	1	1	–41
ν_{17}	3479	3632	3525	583	36	37	1656	123	0	7
ν_{18}	3489	3641	3612	538	35	–30	1657	122	0	7
ν_{19}	3735	3892	3703	94	46	9	2984	1726	97	227
ν_{20}	3739	3896	3703	96	42	20	2989	1723	97	220
ν_{21}	3740	3898	3703	47	88	–36	3133	306	178	–296
ν_{22}							3730	16	37	24
ν_{23}							3730	16	40	21
ν_{24}							3731	14	99	–45

[a] At the MP2/Aug–cc–PVDZ level.[2]

VCD is a strong spectroscopic technique which uses circularly polarized IR light to extract information about AC of chiral molecules. Since different optical isomers absorb different left and right circularly polarized IR light, VCD provides information on the stereo-structure of different enantiomers of a chiral molecule. Different from the IR and Raman spectra, the contributions to VCD spectra of S–$(H_2O)_3$ (Fig. 2(a)) come mostly from the lower-frequency modes, ν_4–ν_{12}. Here, the ν_4–ν_6 modes are the HOH twisting of out-of-plane, ν_7–ν_9 are the HOH rocking in plane, and ν_{10}–ν_{12} are the HOH twisting. Of them, ν_8 is of the largest vibrational rotation strength. In other words, the strongest IR and Raman bands appear in the higher-frequency stretching region (3419–3740 cm^{-1}) whereas the strongest VCD bands are located within the lower-frequency region smaller than 1000 cm^{-1} due to the HOH rocking motions. The VCD spectra are composed of two positive Cotton effects (A and C at nearly 357 and 861 cm^{-1} in Fig. 2(a)) and one negative Cotton effect (B at 572 cm^{-1}).

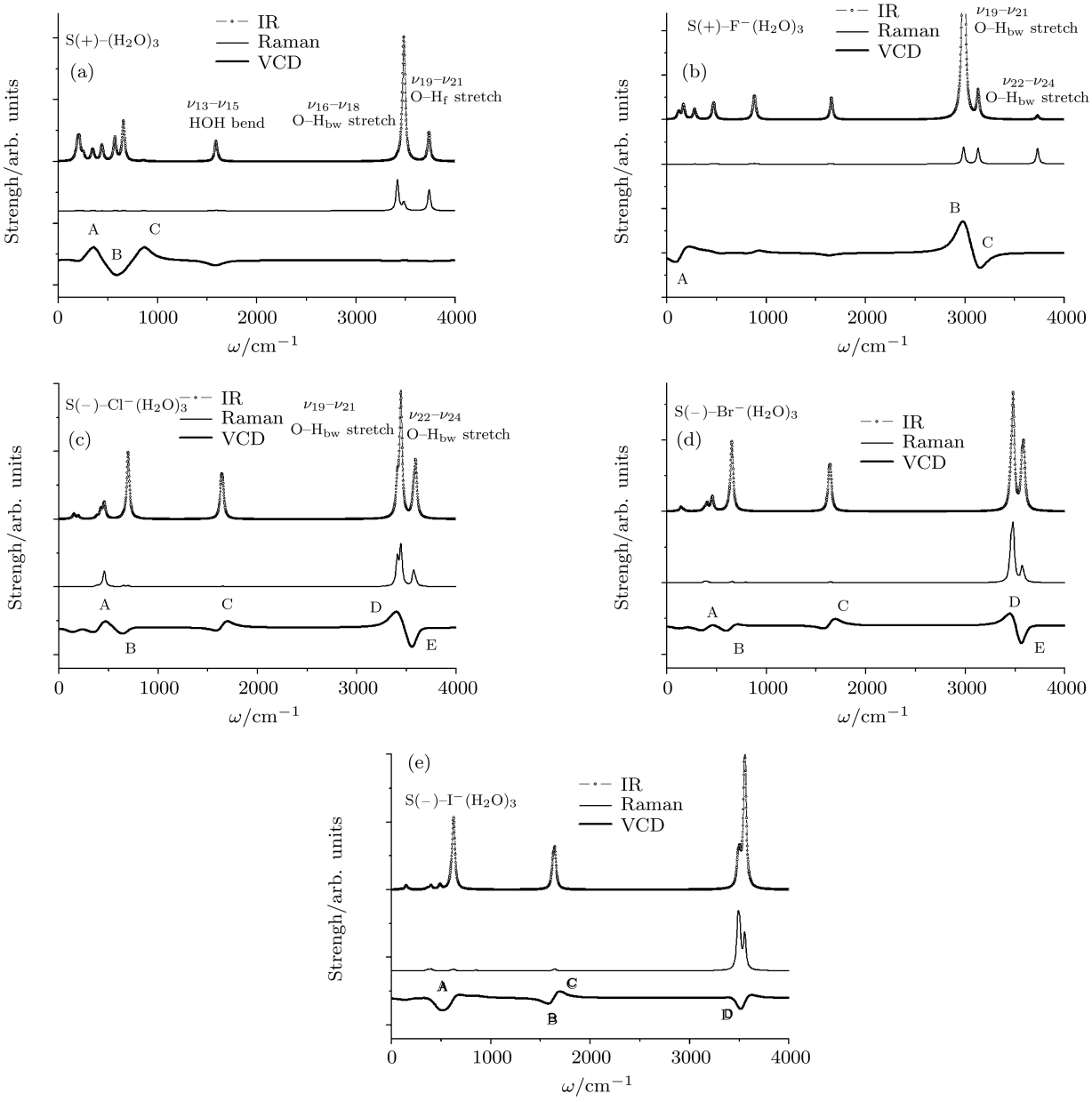


Fig. 2. Simulated IR and Raman and VCD spectra of the S enantiomer by using the fitting of Lorenz's equation with 15-cm^{-1} half-width for the IR and Raman spectra and with 100-cm^{-1} half-width for the VCD spectra.

For quasi-planar $F^-(H_2O)_3$ (Fig. 2(b)), two strongest IR peaks are induced by the ν_{19}–ν_{21} modes. The strongest IR peak at about 2987 cm^{-1} originates from the ν_{19}–ν_{20} asymmetric stretching modes of the O–H_{bx} bond and the second is the result from the ν_{21} symmetric stretching of this bond. The ν_{19}–ν_{24} modes are Raman-active, coming from the O–H_{bw} stretching. In addition to the two Raman peaks at 2987 cm^{-1} and 3133 cm^{-1}, the other Raman peak at 3731 cm^{-1} comes mostly from the ν_{24} mode. Three bands, at about 210, 2987 and 3133 cm^{-1} (A, B, and C), very much contribute to the VCD spectra, and exhibit in turn negative, positive, and negative Cotton effects. The A peak comes from the ν_{21} mode, and the B has its origin in the ν_{19} and ν_{20} modes. Thus, the VCD-active absorptions appear mainly at the higher-frequency range (OH stretching modes), different from the case from HOH rocking modes in $(H_2O)_3$.

For $Cl^-(H_2O)_3$, in 1998 Choi *et al.* measured its IR spectra.[44] We assign the observed vibrational absorptions to the ν_{19}–ν_{24} modes (Table 3). Similar to $F^-(H_2O)_3$, ν_{19}–ν_{21} are the O–H_{bx} stretching, and ν_{22}–ν_{24} are the O–H_{bw} stretching. They give two strong peaks at ∼3593 cm^{-1} and 3444 cm^{-1} (Fig. 2(c)). Unfortunately, previous calculated frequencies (3553, 3581, 3733, 3749 cm^{-1}) at MP2/Aug–cc–PVDZ[5] uniformly overestimate the experimental data (3257, 3357, 3530, 3630 cm^{-1}).[44] Different from the case at the MP2 level, the frequencies (3407, 3444, 3572, 3593 cm^{-1}) at B3LYP/6–311++G(2d,2p) overestimate the experimental lower-frequencies (3257, 3357, 3530 cm^{-1}), and underestimate the experimental higher-frequency (3630 cm^{-1}). Anyway, calculated frequencies at the DFT level are much closer to the experimental data in comparison with the calculated results at the MP2 level.

Table 3. Harmonic vibration frequency (ν, in cm^{-1}), infrared intensity (I, in kM/mol), Raman activity (A, in $Å^4$/amu), and vibrational optical rotatory strength (R, in $\times 10^{-40}$ $esu^2 \cdot cm^2$) of S(–)–$Cl^-(H_2O)_3$ and S(–)–$Br^-(H_2O)_3$ and S(–)–$I^-(H_2O)_3$ calculated at the B3LYP/6–311++G(2d,2p) level, where the harmonic frequency has been scaled by a factor of 0.962.

	S(–)–$Cl^-(H_2O)_3$						S(–)–$Br^-(H_2O)_3$				S(–)–$I^-(H_2O)_3$			
mode	ν	MP2[a]	Expt[44]	I	A	R	ν	IR	A	VCD	ν	I	A	R
ν_1	89	96		1	0	6	82	0	0	3	72	0	0	2
ν_2	90	96		0	0	6	84	0	0	4	81	0	0	2
ν_3	123	128		1	0	–13	102	1	0	–9	90	1	1	–3
ν_4	152	163		18	0	–26	141	15	0	–22	149	15	0	–15
ν_5	153	163		18	0	–26	144	14	0	–21	149	15	0	–16
ν_6	196	207		22	0	37	167	8	0	34	176	2	0	21
ν_7	381	372		9	4	–61	373	7	4	–43	359	6	5	0
ν_8	387	372		7	4	–55	377	7	4	–42	365	5	5	6
ν_9	424	425		65	7	65	404	55	9	55	398	28	14	33
ν_{10}	456	446		59	0	42	456	51	0	12	487	15	0	–51
ν_{11}	460	446		58	0	31	457	50	0	11	491	21	0	–40
ν_{12}	649	661		9	1	–95	623	15	1	–134	600	43	4	–200
ν_{13}	696	708		251	4	27	651	247	4	57	622	276	6	108
ν_{14}	700	708		248	4	20	655	249	4	54	628	269	5	99
ν_{15}	794	804		2	2	2	789	0	3	–3	848	1	6	14
ν_{16}	1636	1676		120	1	–158	1631	100	0	–169	1625	76	2	–178
ν_{17}	1637	1676		120	1	–159	1631	101	0	–170	1626	76	2	–183
ν_{18}	1652	1692		180	2	334	1646	207	6	357	1645	259	11	366
ν_{19}	3407	3553	3257	117	99	77	3457	102	118	–0	3486	155	319	512
ν_{20}	3408	3553	3257	116	98	76	3460	103	118	–4	3502	86	125	–339
ν_{21}	3444	3581	3357	904	291	27	3480	752	344	245	3506	92	120	–367
ν_{22}	3572	3733	3530	142	108	–580	3569	254	95	–785	3554	606	174	–704
ν_{23}	3593	3749	3630	193	19	208	3588	190	17	276	3556	308	60	307
ν_{24}	3594	3749	3630	192	19	208	3588	191	17	275	3556	224	20	576

[a] At MP2/Aug–cc–PVDZ level.[5]

In the IR spectra of S(–)–$Cl^-(H_2O)_3$, five strong absorption peaks are theoretically predicted, at 424–460 cm^{-1} from the O–H_{bw} rocking, 696–700 cm^{-1} from the O–H_{bx} rocking, 1636–1652 cm^{-1} from the O–H_{bw} and O–H_{bx} bending, 3407–3444 cm^{-1} from the O–H_{bx} stretching, and 3572–3594 cm^{-1} from the O–H_{bw} stretching. At the same time, five VCD peaks (A–E in Fig. 2(c)) with positive, negative, positive, positive, and negative Cotton effects appear at 424–460 cm^{-1}, 649 cm^{-1}, 1637 cm^{-1}, 3408 cm^{-1}, and 3572 cm^{-1}, respectively. Compared with S–$F^-(H_2O)_3$, we find that S–$Cl^-(H_2O)_3$ exhibits more VCD-active modes due to the stronger water–water interaction (shorter O–O distance).

For S–$Br^-(H_2O)_3$, the IR and VCD spectra are similar to those in S–$Cl^-(H_2O)_3$ due to the similarity of their geometrical parameters (Table 1). Five absorption peaks appear in the IR spectra. Similar to S–$Cl^-(H_2O)_3$, five VCD peaks (A–E in Fig. 2(d)) have positive, negative, positive, positive, and negative Cotton effects, respectively. Table 3 shows that the vibrational frequencies of this complex are close to those in S–$Cl^-(H_2O)_3$. For example, the strongest mode (3480 cm^{-1}) is a little smaller than that (3444 cm^{-1}) in S–$Cl^-(H_2O)_3$.

For S–$I^-(H_2O)_3$ (Table 3 and Fig. 2(e)), there are four IR peaks. The two highest-energy peaks are very close, originating from the O–H_{bx} stretching (3554 cm^{-1}), and the O–H_{bw} stretching (3486 cm^{-1}), respectively. In the VCD spectra, only one peak is found at ∼3554 cm^{-1}, different from the cases in other complexes containing two remarkable Cotton effects in high-frequency range. The cause is that the optical rotatory strength at 3486 cm^{-1} is much weaker than that at 3554 cm^{-1}. The Raman spectra has two strong peaks from the O–H_{bx} stretching (3554 cm^{-1}) and the O–H_{bw} stretching (3486 cm^{-1}). Since the Raman spectra of S–$F^-(H_2O)_3$ have three peaks in the high-frequency range, this cluster is similar to S–$Cl^-(H_2O)_3$ and S–$Br^-(H_2O)_3$, different from S–$F^-(H_2O)_3$.

3.3. Optical rotatory power (ORP)

Recently, *ab initio* molecular orbital calculations of the optical rotatory response of a single oriented water molecule among a limited number of excited states have been reported at the CCSD/6–311+G(d,p) level.[45] It was found that optical rotations have their important origin in the relative dispositions of the transition moments with respect to the wave-vectors and excitations.

For our clusters, the calculated ORP in different solvents in terms of the PCM model[36] at B3LYP/6–311++G(2d,2p) and B3LYP/Aug–cc–pVTZ are collected in Table 4. Static ORP, $[\alpha]_{D0}$ in vacuum, is used to determine the optical rotation direction of the S enantiomer. We notice that static ORP are positive for S–$(H_2O)_3$ and S–$F^-(H_2O)_3$, and negative for S–$X^-(H_2O)_3$ (X = Cl, Br, I) at B3LYP/6–311++G(2d,2p). Thus, absolute configuration with different optical rotational directions is denoted as S(+)–$(H_2O)_3$, S(+)–$F^-(H_2O)_3$, and S(–)–$X^-(H_2O)_3$ (X = Cl, Br, I), respectively. After the water trimer combines with the fluoride ion, F^-, the optical rotational direction is not changed. However, for the complexation of the water trimer with the other halide ions (Cl^-, Br^-, I^-), the ORP is altered in sign from positive to negative.

For S(+)–$(H_2O)_3$, the solvent and frequency effects enhance chirality since $[\alpha]_{D0}$ is 3.43° in vacuum, 3.90° in argon, 4.42° in CCl_4, 5.23° in water, and $[\alpha]_D$ is 4.90° in vacuum, 5.54° in argon, 6.26° in CCl_4, 9.09° in water at B3LYP/6–311++G(2d,2p). $[\alpha]_{D0}$ and $[\alpha]_D$ at B3LYP/Aug–cc–pVTZ are smaller than those at B3LYP/6–311++G(2d,2p) due to the basis set effect.

Different from the case in S(+)–$(H_2O)_3$, the solvent and frequency effects of S(+)–$F^-(H_2O)_3$ reduce the magnitudes of the optical rotation. Concretely, $[\alpha]_{D0}$ is changed from 12.09° in vacuum to 5.24° in water, and $[\alpha]_D$ is reduced from 11.37° in vacuum to 4.87° in water at B3LYP/6–311++G(2d,2p). In addition, calculated $[\alpha]_{D0}$ and $[\alpha]_D$ at B3LYP/Aug–cc–pVTZ are almost twice as large as those at B3LYP/6–311++G(2d,2p).

For S(–)–$Cl^-(H_2O)_3$, $[\alpha]_{D0}$ and $[\alpha]_D$ at B3LYP/6–311++G(2d,2p) and B3LYP/Aug–cc–pVTZ are almost equal in vacuum and water. With an augmentation of dielectric constant from vacuum to water, the ORP becomes more negative. For example, $[\alpha]_{D0}$ at B3LYP/6–311++G(2d,2p) is –1.53° in vacuum and –17.06° in water.

For S(–)–$Br^-(H_2O)_3$, $[\alpha]_{D0}$ and $[\alpha]_D$ at B3LYP/6–311++G(2d,2p) are much larger than those at B3LYP/Aug–cc–pVTZ. On the other hand, the frequency effect in water reduces the ORP from –16.19° to –7.13° at B3LYP/6–311++G(2d,2p), whereas the difference between $[\alpha]_{D0}$ and $[\alpha]_D$ is small in CCl_4 and Ar and vacuum.

For S(–)–$I^-(H_2O)_3$, the ORP at B3LYP/6–311++G(2d,2p) is close to that at B3LYP/Aug–cc–pVTZ, smaller than those in S(–)–$Cl^-(H_2O)_3$ and S(–)–$Br^-(H_2O)_3$. Similarly, the solvent effect enhances the negative value of the ORP, and the frequency effect reduces the negative value of the ORP.

In sum, the solvent effect enhances the negative chirality of S(–)–$X^-(H_2O)_3$ (X = Cl, Br, I) since the negative ORP is in the order of $[\alpha]_{D0}$ (water) > $[\alpha]_{D0}$ (CCl_4) > $[\alpha]_{D0}$ (Ar) > $[\alpha]_{D0}$ (vacuum). For S(–)–$F^-(H_2O)_3$, the solvent effect reduces its positive ORP, along with the series $[\alpha]_{D0}$ (water) < $[\alpha]_{D0}$ (CCl_4) < $[\alpha]_{D0}$ (Ar) < $[\alpha]_{D0}$ (vacuum). For S(–)–$(H_2O)_3$, the solvent effect enhances its positive ORP as $[\alpha]_{D0}$ (water) > $[\alpha]_{D0}$ (CCl_4) > $[\alpha]_{D0}$ (Ar) > $[\alpha]_{D0}$ (vacuum).

Table 4. Calculated optical rotatory power (ORP) (in degrees) in different solvents according to the PCM model.

solvent	water (ε=78.39)		CCl_4 (ε=2.228)		Ar (ε=1.43)		vacuum (ε=1.00)	
	$[\alpha]_{D0}$	$[\alpha]_D$	$[\alpha]_{D0}$	$[\alpha]_D$	$[\alpha]_{D0}$	$[\alpha]_D$	$[\alpha]_{D0}$	$[\alpha]_D$
B3LYP/6–311++G(2d,2p)								
S(+)–$(H_2O)_3$	5.23	9.09	4.42	6.26	3.90	5.54	3.43	4.90
S(+)–$F^-(H_2O)_3$	5.24	4.87	9.77	8.50	11.80	10.74	12.09	11.37
S(–)–$Cl^-(H_2O)_3$	–17.06	–6.39	–6.65	–7.36	–3.74	–4.50	–1.53	–2.12
S(–)–$Br^-(H_2O)_3$	–16.19	–7.13	–9.59	–10.01	–8.62	–9.12	–8.66	–9.08
S(–)–$I^-(H_2O)_3$	–12.55	–2.40	–4.09	–3.23	–2.60	–1.63	–1.86	–0.60
B3LYP/Aug–cc–pVTZ								
S(+)–$(H_2O)_3$	3.98	3.61	0.76	2.22	–0.13	1.19	–0.83	0.30
S(+)–$F^-(H_2O)_3$	9.88	12.91	19.96	20.06	23.00	23.76	24.66	26.44
S(–)–$Cl^-(H_2O)_3$	–16.97	–7.23	–7.31	–7.36	–4.23	–4.26	–1.71	–1.45
S(–)–$Br^-(H_2O)_3$	–9.99	–3.62	–4.46	–3.94	–2.69	–2.11	–1.26	–0.44
S(–)–$I^-(H_2O)_3$	–9.43	–3.38	–4.43	–3.38	–2.78	–1.47	–1.19	0.73

4. Conclusion

In the present paper, we have determined the ACs and chiral optical properties of the water trimer and its halide clusters at the DFT-B3LYP level. The IR, Raman and VCD spectra are assigned on the basis of an analysis of harmonic vibrational modes. For the water trimer, it is found that chirality depends mostly on the O–H rocking. For halide–water clusters, the O–H stretching is more important in the chiral origin. In addition, it is predicted that S–$(H_2O)_3$ and S–$F^-(H_2O)_3$ are positively chiral, and S–$X^-(H_2O)_3$ (X = Cl, Br, I) are negatively chiral. Furthermore, the values and sign of the ORP can be modulated by changes of solvent and incident light frequency. It is found that the charge transfer magnitude of the halide ion and the frequency difference between the O–H_{bw} and O–H_{bx} stretching modes are in turn reduced with the addition of the halogen atomic number.

References

[1] Pugliano N and Saykally R J 1992 *Science* **257** 1937

[2] Xantheas S S and Dunning Jr T H J 1993 *J. Chem. Phys.* **99** 8774

[3] Wales D J and Hodges M P 1998 *Chem. Phys. Lett.* **286** 65

[4] Baik J, Kim J, Majumdar D and Kim K S 1999 *J. Chem. Phys.* **110** 9116

[5] Xantheas S S 1996 *J. Phys. Chem.* **100** 9703

[6] Lee H M and Kim K S 2001 *J. Chem. Phys.* **114** 4461

[7] Lee H M, Suh S B and Kim K S 2003 *J. Chem. Phys.* **119** 7685

[8] Merrill G N and Webb S P 2003 *J. Phys. Chem.* A **107** 7852

[9] Feller D, Glendening E D and Woon D E 1995 *J. Chem. Phys.* **103** 3526

[10] Glendening E D and Feller D 1995 *J. Phys. Chem.* **99** 3060

[11] Feller D 1997 *J. Phys. Chem.* A **101** 2723

[12] Lee H M, Kim J K, Lee S, Mhin B J and Kim K S 1999 *J. Chem. Phys.* **111** 3995

[13] Gruenloh C J, Carney J R, Arrington C A, Zwier T S, Fredericks S Y and Jordan K D 1997 *Science* **276** 1678

[14] Miyazaki M, Fujii A and Mikami N 2004 *J. Phys. Chem.* A **108** 8269

[15] Liu Y, Peng C D, Lan X F, Luo X S, Shen Z H, Lu J and Ni X W 2005 *Acta Phys. Sin.* **54** 5455 (in Chinese)
[16] Alkorata I, Zborowski K and Elguero J 2006 *Chem. Phys. Lett.* **427** 289
[17] Alkorata I and Elguero J 2002 *J. Chem. Phys.* **117** 6463
[18] Alkorata I, Elguero J and Zborowski K J 2007 *J. Phys. Chem.* A **111** 1096
[19] Zborowski K, Proniewcz L M, Alkorata I and Elguero J 2005 *Chem. Phys. Lett.* **409** 163
[20] Perdew J P 1986 *Phys. Rev.* B **33** 8822
[21] Lee C, Yang W and Parr R G 1988 *Phys. Rev.* B **37** 785
[22] Miehlich B, Savin A, Stoll H and Preuss H 1989 *Chem. Phys. Lett.* **157** 200
[23] Vosko S H, Wilk L and Nusair M 1980 *Can. J. Phys.* **58** 1200
[24] Krishnan R, Binkley J S, Seeger R and Pople J A 1980 *J. Chem. Phys.* **72** 650
[25] laudeau J P, McGrath M P, Curtiss L A and Radom L 1997 *J. Chem. Phys.* **107** 5016
[26] Clark T, Chandrasekhar J and Schleyer P V R 1983 *J. Comp. Chem.* **4** 294
[27] Dunning Jr T H 1989 *J. Chem. Phys.* **90** 1007
[28] Woon D E and Dunning Jr T H 1994 *J. Chem. Phys.* **100** 2975
[29] Kendall R A, Dunning Jr T H and Harrison R J 1992 *J. Chem. Phys.* **96** 6796
[30] Woon D E and Dunning Jr T H 1993 *J. Chem. Phys.* **98** 1358
[31] Wilson A K, Woon D E, Peterson K A and Dunning Jr T H 1999 *J. Chem. Phys.* **110** 7667
[32] Peterson K A, Figgen D, Goll E, Stoll H and Dolg M 2003 *J. Chem. Phys.* **119** 11113
[33] Frisch M J, Trucks G W, Schlegel H B, Scuseria G E, Robb M A, Cheeseman J R, Montgomery J A, Vreven Jr T, Kudin K N, Burant J C, Millam J M, Iyengar S S, Tomasi J, Barone V, Mennucci B, Cossi M, Scalmani G, Rega N, Petersson G A, Nakatsuji H, Hada M, Ehara M, Toyota K, Fukuda R, Hasegawa J, Ishida M, Nakajima T, Honda Y, Kitao O, Nakai H, Klene M, Li X, Knox J E, Hratchian H P, Cross J B, Adamo C, Jaramillo J, Gomperts R, Stratmann R E, Yazyev O, Austin A J, Cammi R, Pomelli C, Ochterski J W, Ayala P Y, Morokuma K, Voth G A, Salvador P, Dannenberg J J, Zakrzewski V G, Dapprich S, Daniels A D, Strain M C, Farkas O, Malick D K, Rabuck A D, Raghavachari K, Foresman J B, Ortiz J V, Cui Q, Baboul A G, Clifford S, Cioslowski J, Stefanov B B, Liu G, Liashenko A, Piskorz P, Komaromi I, Martin R L, Fox D J, Keith T, Al-Laham M A, Peng C Y, Nanayakkara A, Challacombe M, Gill P M W, Johnson B, Chen W, Wong M W, Gonzalez C and Pople J A 2003 *Gaussian* 03 (Revision B.05) (Pittsburgh P A: Gaussian Inc.)
[34] SImonato J P, Pecaut J and Marchon J C 1998 *J. Am. Chem. Soc.* **120** 7363
[35] Toronto D, Aarrazin F, Pecaut J, Marchon J C, Shang M and Scheidt W R 1998 *Inorg. Chem.* **37** 526
[36] Miertus S, Scrocco E and Tomasi J 1981 *J. Chem. Phys.* **55** 117
[37] Zhang S L, Chen H S, Yan S and Yin Y H 2007 *Acta Phys. Sin.* **56** 2553 (in Chinese)
[38] Mo O, Yanez M and Elguero J 1992 *J. Chem. Phys.* **97** 6628
[39] Kim J, Lee H M, Suh S B, Majumdar D and Kim K S 2000 *J. Chem. Phys.* **113** 5259
[40] Xantheas S S and Dunning Jr T H 1994 *J. Phys. Chem.* **98** 13489
[41] Liu H T and Li J M 2005 *Chin. Phys.* **14** 1974
[42] Zhang C R, Chen H S, Song Y and Xu G J 2007 *Chin. Phys.* **16** 2394
[43] Bentwood R M, Barnes A J and Orville-Thomas W J 1980 *J. Mol. Spectrosc.* **84** 391
[44] Choi J O, Kuwata K T, Cao Y B and Okumura M 1998 *J. Phys. Chem.* A **102** 503
[45] Isborn C, Claborn K and Kahr B 2007 *J. Phys. Chem.* A **111** 7800